Progress In Electromagnetics Research M, Vol. 62, 79–88, 2017

A Compact CPW Fed UWB Antenna with Quad Band Notch Characteristics for ISM Band Applications

Raed Abdulkareem Abdulhasan*, Rozlan Alias, and Khairun Nidzam Ramli

Abstract—A quad band-notched compact ultra-wideband (UWB) patch antenna to operate on the industry, scientific, and medical (ISM) bands are presented in this study. A modified hexagonal patch vertex-fed with a coplanar waveguide (CPW) is fabricated on an FR-4 substrate with size of $43 \times 28 \times 1.6\,\text{mm}^3$ and fractional bandwidth of 133%. The compact antenna operates at a frequency of 2.45 GHz, which is often required for the efficient performance of ISM utilisation. The existing bands share the same bandwidth as that of UWB systems. Therefore, a notched band at 3 GHz for worldwide interoperability for microwave access (WiMAX), and a further resonance band at 2.45 GHz for ISM are generated by implementing a meander-line strip on the antenna. Furthermore, the design demonstrates a couple of F-shaped slots and an inverted diamond-shaped slot on the patch. Moreover, a pair of J-shaped slots is loaded on the ground plane. The downlink C-band, wireless local area network (WLAN), and downlink X-band are rejected by the proposed slots, respectively. The current distribution, gain, radiation efficiency, and quad notched parameters of the proposed antenna are studied by using CST software. The demonstrated prototype covers an ISM band at (2.2 GHz–2.6 GHz) with a return loss of -23.45 dB and omnidirectional radiation patterns. A good agreement is observed between measured and the simulated results. This paper has presented a solution for both interference and miniaturised issues.

1. INTRODUCTION

In recent years, the UWB spectrum has become attractive in wireless connection systems. In 2002, the Federal Communication Commission (FCC) gave license to propagate signals in the UWB spectrum (3.1 GHz–10.6 GHz) with a fractional bandwidth (FBW) of more than 100% for civilian communication applications [1]. The UWB systems have many advantages, such as low operating power, high data rate, and low profile. Therefore, one of the critical components in UWB systems is the antenna, which should have good impedance matching with all UWB spectrum frequencies. Consequently, several techniques on antenna structures have been developed to obtain impedance matching with UWB bandwidth.

Printed monopole UWB patch antenna is commonly used for UWB portable devices. The advantages of a printed UWB patch antenna are attributed to its low profile, easy fabrication, lightweight, low cost, and omnidirectional radiation patterns [2, 3]. Furthermore, a UWB patch antenna can be connected to a port connector by using different fed line techniques such as microstrip-fed line [4], transformer microstrip-fed line [5], and CPW [6]. These techniques are employed with a finite ground plane to achieve UWB bandwidth.

However, some traditional bands for different wireless communication systems exist over the UWB spectrum frequencies. For example, downlink satellite communication X-band 7.5 GHz [7], WLAN 5.8 GHz [7, 8] downlink C-band 4 GHz [9], and WiMAX 3.2 GHz [8, 10] share the same bandwidth as

Received 8 September 2017, Accepted 28 October 2017, Scheduled 9 November 2017

* Corresponding author: Raed Abdulkareem Abdulhasan (raadabd39@gmail.com).

The authors are with the Department of Communication Engineering, Faculty of Electrical and Electronic Engineering, Universiti Tun Hussein Onn Malaysia, Parit Raja, Batu Pahat, Johor 86400, Malaysia.

UWB systems. These bands cause electromagnetic interference (EMI) with UWB systems. Usually, installing RF filters in communication devices increases the systems operation power, complexity, and size. In contrast, adding notch filters on a UWB antenna can solve this problem. A notch filter has several advantages such as being easy to fabricate, less complexity, relatively inexpensive, and reliable. Moreover, multi-band rejection is required on the same antenna to overcome the EMI with several existing bands. Consequently, some UWB antennas are introduced with different notch structures. For example, C-shaped [7], U-shaped [8] and L-shaped [9] notches are proposed on UWB antennas.

Practically, a small UWB antenna is required for portable communication devices. However, the ISM band is utilised for several applications at 2.45 GHz. For example, microwave ovens, diathermy machines, wireless computers, and wireless sensor networks are operated at the 2.4–2.5 GHz band [11–13]. The size of a typical ISM band patch antenna is quite large ($\lambda_g/4$) with a full ground plane on the back layer, which increases the fabrication cost. Moreover, an ISM band patch antenna has a narrow bandwidth and single direction radiation pattern. The efficiency of the antenna design and compact size are introduced for the ISM band. A solution for miniaturising both the antenna size and the interference between the existing bands and UWB systems spectrum is introduced in this study. By reducing manufacturing costs, utilising advantages (for ISM applications) of the UWB patch antennas, producing a unique plane small antenna, and with an omnidirectional radiation pattern for portable devices will help to resolve these problems.

In this paper, loading four notches on a compact UWB unique plane patch antenna is demonstrated using quad rejection bands and further resonance band for ISM applications. A solution of the two common research challenges on antenna design (EMI and miniaturised antenna size) is introduced in this study. The following sections are covered in this study. In Section 2, the entire UWB bandwidth (2.8 GHz–14 GHz) is achieved by implementing a CPW vertex-fed hexagonal monopole UWB antenna. In Section 3, implementing the four band notches in a special process entirely rejected UWB bandwidth is presented, and Section 4 discusses the effect of varying the notches parameters. Section 5 compares the simulation and measurement results and also includes the investigation of distributed current, radiation pattern, gain, and radiation efficiency of the proposed antenna at notched frequencies. The last section of the study presents the overall conclusion that the applied method utilises a unique-plane UWB antenna and quad-notch characteristics, thereby demonstrating that the compact size antenna operates at the ISM band.

2. ANTENNA DESIGN

The compact CPW-fed hexagonal monopole UWB antenna is displayed in Figure 1. The proposed antenna is printed on a single plane of an FR-4 substrate with thickness (H). The strip fed line has a selected length (L_f), width (W_f), and gap (S_{cpw}) to achieve the impedance of 50 Ω for the whole UWB bandwidth. The radiated patch, CPW-fed antenna, and two ground plates are printed on the top layer of the substrate to improve the antenna bandwidth and miniaturise the antenna size.

Based on the two different configurations of a printed hexagonal monopole antenna (PHMA) [14], the side-fed connection (PHMAS) is considered as a reference design (Antenna 1). CPW is utilised in this design to improve the antenna bandwidth and introduce a unique plane structure. The PHMAS (Antenna 1) achieves a bandwidth of (3.3 GHz to 10.2 GHz) with side lengths (S) of 8.5 mm (see Figure 2). Referring to Equation (1) [14], increasing the radiation patch size and the feed line length can decrease the lower resonance frequency (F_L). However, these parameters will also increase the overall size of the antenna. Therefore, the following process is considered to make F_L less than 3.1 GHz with a compact size. First, the patch of PHMAS (Antenna 1) is rotated by 60° to create a vertex-fed connection between the feed line and the radiation patch. At this point, the total length of the patch (L) is increased without increasing the length of the sides, which can be calculated by $[L = 2 \times S]$ with $a = 30°$ for the printed hexagonal monopole antenna with vertex-feed (PHMAV) [14]. Moreover, the feed line length ρ is defined as a form of multiple adjacent resonances based on the patch impedance matching. The mechanism of providing UWB antenna bandwidth is achieved by obtaining the finite ground plane and gap ρ parameters. The optimum value of $\rho = 0.5$ mm for PHMAV offers a higher bandwidth than PHMAS because of the patch shape which has a better transition of input impedance at F_L and higher frequency (F_H). Next, the final antenna structure in Figure 1(b) is implemented by

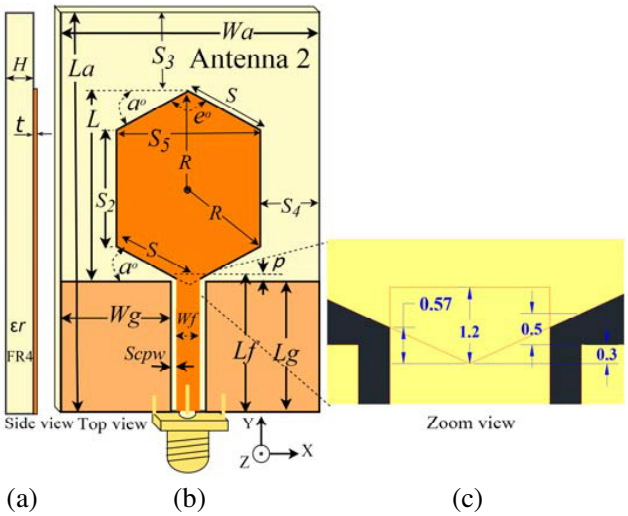

Figure 1. Antenna structure without notches.

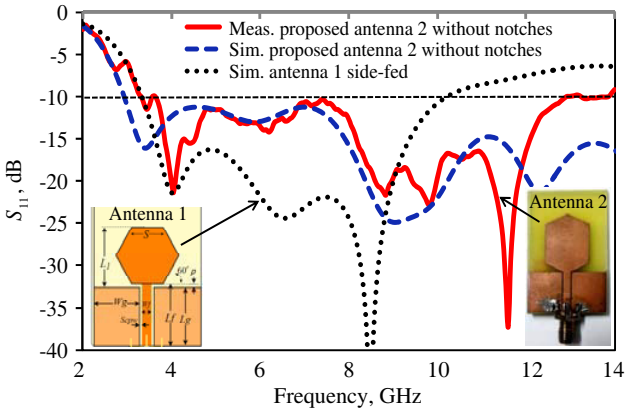

Figure 2. Measurement and simulation S_{11}.

obtaining the optimum value of angle $a = 24°$ and increasing both left and right patch sides (S_2) to 14 mm to improve the input impedance at F_L and F_H, respectively. These steps achieve the entire antenna FBW of 133% (2.8 GHz–14 GHz) for both the upper and lower frequencies as illustrated in Figure 2 (Antenna 2). The lower resonance frequency (F_L) of the proposed design is developed based on the modified formula for the cylindrical monopole antenna as [14]:

$$F_L\,(\text{GHz}) = c/\lambda = 7.2/(L + r + \rho) \times K' \tag{1}$$

where L is the total height of the demonstrated radiation patch, r the effective radius of the equivalent cylindrical monopole antenna in (cm) [14], ρ the feed line in (cm), and the constant $k' = 1.15$ represents the empirical value for effective dielectrics of the FR-4 substrate. Since the proposed patch structure has $a \neq 30°$, and the lengths of the six sides are not equal. The calculation equations of both L and r are derived concerning the proposed patch radius (R) as:

$$L = 2 \times R, \quad r = (2 \times R \times \sin a \times \cos^3 a)/\pi, \text{ and } R = S/(2 \times \sin a) \tag{2}$$

The demonstrated compact UWB antenna is simulated and measured by using CST Microwave Studio, and Vector Network Analyser R&S ZVA14, respectively. The tested results illustrate a broad bandwidth from 3.1 GHz to 14 GHz. Figure 2 presents the return loss S_{11} for both the simulation and measurement results of the demonstrated antenna. The antenna parameters are shown in Figures 1(a), 1(b) and 1(c) ($W_a = 28$ mm, $L_a = 43$ mm, $H = 1.6$ mm, $\varepsilon_r = 4.3$, $\tan\delta = 0.018$, $S = 8.5$ mm, $S_2 = 14$ mm, $S_3 = 8.2$ mm, $S_4 = 6.2$ mm, $S_5 = 15.5$ mm, $L = 20.7$ mm, $t = 0.035$ mm, $W_f = 2.54$ mm, $L_f = 14.3$ mm, $W_g = 12.2$ mm, $L_g = 14$ mm, $\rho = 0.5$ mm, $S_{cpw} = 0.5$ mm, $e = 132°$, $R = 10.5$ mm, and $a = 24°$).

3. NOTCHED BANDS

In this section, four notched bands are introduced on the proposed antenna to avoid the EMI with WiMAX, WLAN, downlink C-band, and X-band systems. The demonstrated antenna with quad notched bands is presented in a single plane as displayed in Figure 3(a). Moreover, Figure 3(b) illustrates the proposed four-notch structure and parameters. The meander-line strip achieves the first rejected band at the centre frequency of 3.1 GHz. This copper strip has parameters, which are horizontal length (L_s) of 7 mm, vertical length (Z_s) of 1 mm, and strip width (T_{ms}) of 0.5 mm. The strip is located at the upper edge of the radiation patch to achieve band-notch characteristics. At this location, the strip is interrupted by the propagated signal. The total length of the strip can be calculated to reject the frequency at a half guided wavelength [4]:

$$L_{ms} = \text{Notch length} \approx c/2 \times F_{\text{notch}} \times \sqrt{\varepsilon_{reff}} \tag{3}$$

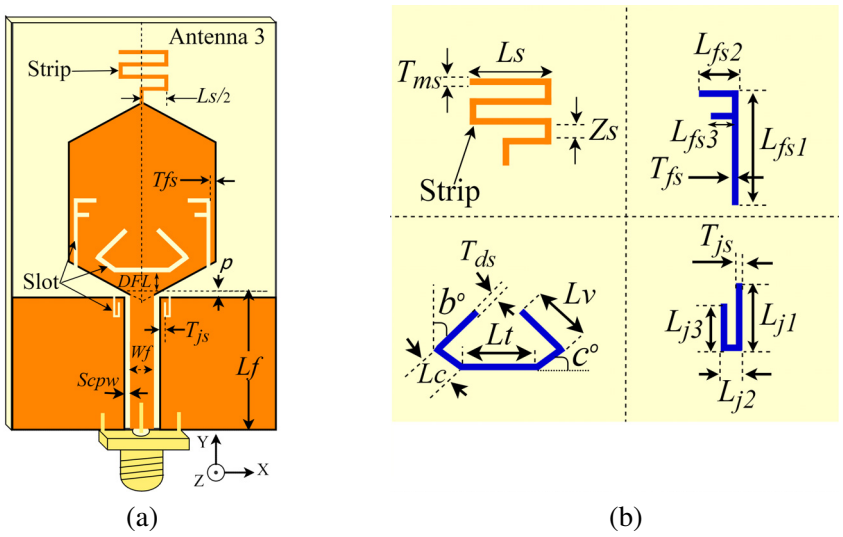

Figure 3. (a) The top layer of UWB antenna with four notches, (b) the four notches structure.

$$\varepsilon_{reff} = (\varepsilon_r + 1)/2 \tag{4}$$

$$L_{ms} = (3.5 \times L_S) + (4 \times Z_S) + T_{ms} \tag{5}$$

where F_{notch} is the notch frequency and c the speed of light. The shortest path of the meander-line L_{ms} is calculated by applying Equation (5), and the effective dielectric constant (ε_{reff}) is calculated by using Equation (4) [6].

The second rejected band is achieved at 4 GHz by loading a symmetrical couple of F-shaped slots on the radiation patch. The F-shaped slot structure is illustrated in Figure 3(b). These slots have symmetrical dimensions and positions, which are $Lfs1$ of 8.2 mm, $Lfs2$ of 3 mm, $Lfs3$ of 2 mm, and width of slots (T_{fs}) of 0.5 mm. The couple of F-slots acts as a quarter guided wavelength band-stop filter. The centre notched band is obtained by using Equation (6) [6]. Moreover, the total length of the couple of F-slots (Lfs) is calculated and optimised by using Equation (7) [4].

$$\text{Notch length}(L_{fs}) \approx c/4 \times f_{\text{notch}}\sqrt{\varepsilon_{eff}} \tag{6}$$

$$L_{fs} = L_{fs1} + L_{fs2} + L_{fs3} - (2 \times T_{fs}) \tag{7}$$

Next, the third notched band at 5.8 GHz is obtained by cutting the inverted diamond slot on the radiation patch as displayed in Figure 3(b). The diamond slot parameters are presented in Figure 3(b) as the table length (L_t) of 6 mm, crown lengths (L_c) of 2.5 mm, crown angle ($c°$) of 36°, pavilion length (L_v) of 4 mm, pavilion angle ($b°$) of 50°, and slot width (T_{ds}) of 0.5 mm. The inverted diamond closed-end slot acts as a half-guided wavelength band-stop filter. The centre notched band is obtained by applying Equation (3). Furthermore, the total length of the diamond slot (L_{ds}) is calculated by using Equation (8) [4]:

$$L_{ds} = (2L_v + 2L_c + L_t + 2T_{ds}) \tag{8}$$

The fourth notched band is achieved by cutting a pair of J-shaped open-end slots on the ground plane. The pair of J-slot generates a quarter-guided wavelength band-stop filter at the X-band. Figure 3(b) illustrates the J-slot structure and parameters. The two J-slots have optimum parameters, which are slot lengths $L_{j1} = 2.6$ mm, $L_{j2} = 1.5$ mm, $L_{j3} = 2.1$ mm, and slot width $T_{js} = 0.5$ mm. The centre notched frequency is obtained by using Equation (6). Furthermore, the total length of the pair of J-slot (L_{js}) is calculated by using Equation (9) [4]:

$$L_{Js} = L_{J1} + L_{J2} + L_{J3} - (2 \times T_{Js}) \tag{9}$$

4. PARAMETRIC STUDY

The meander-line strip is the first presented notch at (2.76 GHz–3.4 GHz). The simulation results of changing the L_s length with a fixed Z_s of 1 mm is illustrated in Figure 4. The centre notched band is

notably shifted from 3.2 GHz to 2.85 GHz with a significant improvement of the VSWR magnitude from 4.7 to 13.04 by increasing the length of L_s from 6 mm to 8 mm, respectively. The proposed antenna is introduced with an optimum strip length L_s of 7 mm. The variation of the meander-line strip height Z_s by setting the parameter L_s of 7 mm is displayed in Figure 5. Increasing parameter Z_s from 0.5 mm to 1.5 mm of the meander-line strip slightly shifts the centre notched frequency from 3.2 GHz to 2.9 GHz with a significant improvement of the VSWR magnitude from 2.7 to 11.2, respectively. By decreasing both L_s and Z_s to 6 mm, and 0.5 mm, respectively, the first notched band is omitted at 3.2 GHz. Therefore, the optimum length of L_s = 7 mm and Z_s = 1 mm are selected to achieve the notched frequency at 3 GHz based on Equations (3) and (5). Furthermore, the meander-line strip proves a new resonance frequency at 2.45 GHz for ISM applications.

Figure 6 presents the study for varying L_{fs1} parameter of the couple of F-notches. The validation is made among L_{fs1} = 7 mm, 8.2 mm, and 9 mm. When L_{fs1} = 7 mm, the study shows a good notched band VSWR of 11.59 at the band (3.8 GHz–5 GHz). Increasing the F-notch length L_{fs1} to 9 mm shifts the notched band (3.3 GHz–4.2 GHz) to the higher frequency without displaying any improvement on the VSWR magnitude. The couple of F-slots with a width (T_{fs}) is simulated in Figure 7 displaying the varying values of 0.3 mm, 0.5 mm, and 0.8 mm. When T_{fs} = 0.8 mm, both the VSWR magnitude of 15.3 and the notched bandwidth of (3.6–4.7 GHz) are improved. However, this increment thereby reduces the rejection magnitude of the meander-line strip. Therefore, the optimum couple of F-slot parameters L_{fs1} = 8.2 mm and T_{fs} = 0.5 mm are chosen to achieve the rejected band at 4 GHz.

The comparison results among the different diamond slot locations are displayed in Figure 8. When the distance between the feed line and the diamond slot (DFL) = 1 mm, the results show significant improvement of the rejection VSWR magnitude of 9 with a bandwidth of 5–6.5 GHz. Moreover,

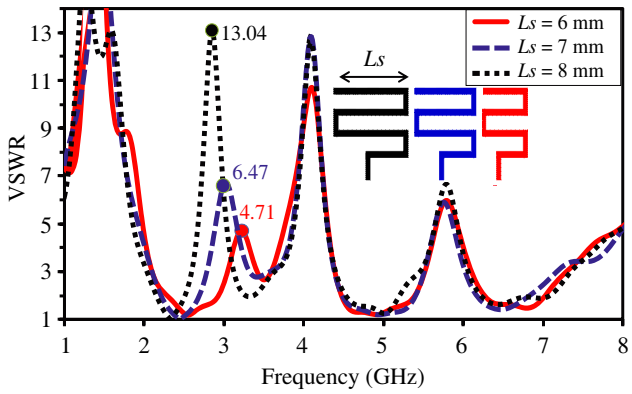

Figure 4. Variation of (L_s).

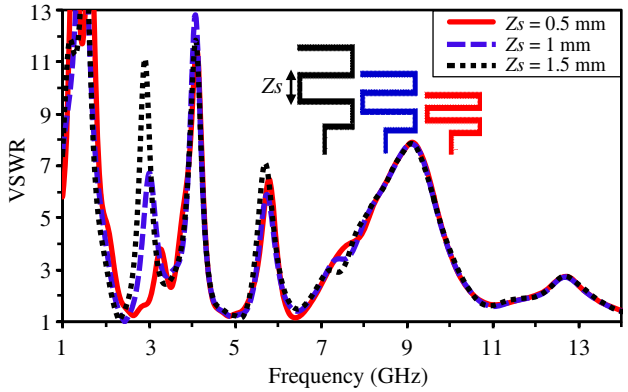

Figure 5. Variation of (Z_s).

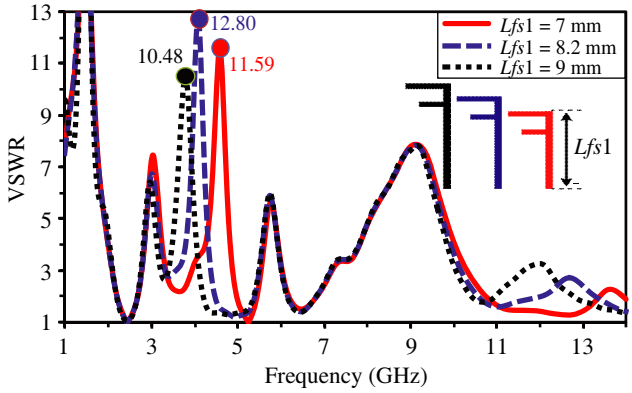

Figure 6. Variation of (L_{fs1}).

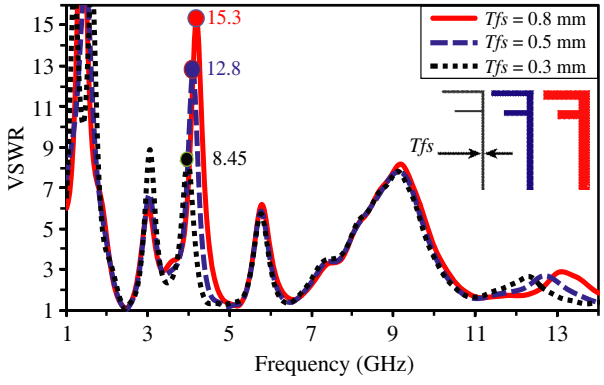

Figure 7. Changing of (T_{fs}).

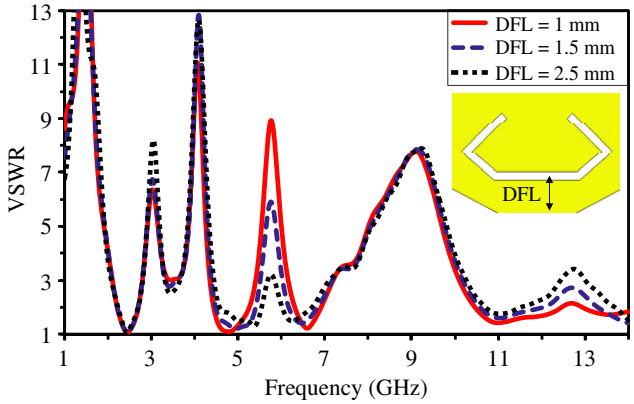

Figure 8. Changing of (DFL).

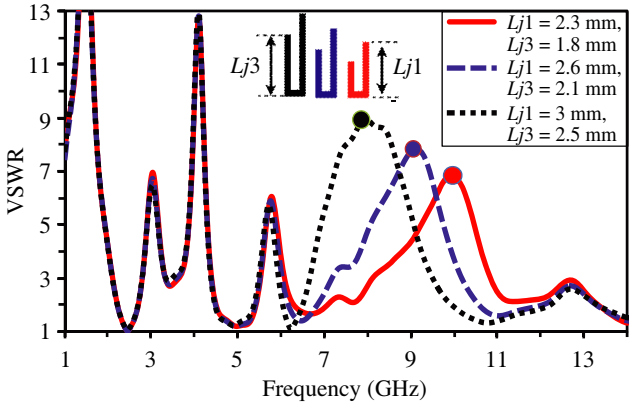

Figure 9. Changing of (L_{j1}, L_{j3}).

the produced rejection harmonic at 12.7 GHz is omitted. This modification decreases the rejection magnitude at both 3 GHz and 4.1 GHz. Therefore, the optimum value of $DFL = 1.5$ mm is selected for the demonstrated structure.

Both the parameters L_{j1} and L_{j3} of the pair of J-slots are studied by varying their lengths as displayed in Figure 9. The validation is shown by setting both $L_{j1} = 2.3$ mm, 2.6 mm, and 3 mm and $L_{j3} = 1.8$ mm, 2.1 mm, and 2.5 mm at the same time. Increasing both lengths L_{j1} to 3 mm and L_{j3} to 2.5 mm achieves a higher VSWR magnitude of 9, shifting the rejection band to (6.5 GHz–9.9 GHz). Therefore, $L_{j1} = 2.6$ mm and $L_{j3} = 2.1$ mm are chosen for the proposed structure to achieve band rejection at 9 GHz.

From the above discussion, the notch length is selected around $\lambda_g/2$ for the closed-end notch and $\lambda_g/4$ for the open-end notch. In other words, increasing the notch length shifts the centre notched band to a lower frequency. However, decreasing the notch length shifts the rejected band to a higher frequency. Changing the notch length is seen to tune the operating frequency of the notch filter. Conversely, increasing the notch width shifts the notched band to the higher frequency and increases the notch bandwidth. The effect of changing the notch width is as tuning the capacitance of an equivalent notch parallel RLC branch. Moreover, reducing the distance between the notch and the feed line is observed as a significant improvement of both the VSWR rejection magnitude and the rejection bandwidth of the unchanging notched band. Therefore, adjusting the notch length affects the F_{notch}, but changing the notch location affects the bandwidth and the rejection quality. In short, the rejection band can be controlled by arranging the notch structure and position.

5. RESULTS AND DISCUSSION

The measured return loss of the demonstrated antenna without notches is tested. The collected test data from the demonstrated design and the simulated result are in good agreement as shown in Figure 10. Moreover, Figure 11 shows the simulation and measurement of the VSWR comparison of the proposed antenna with quad rejected bands. The measured result exhibits a VSWR higher than 2 to reject the WiMAX, C-band, WLAN, and X-band at (2.7 GHz–3.4 GHz), (3.4 GHz–4.5 GHz), (5.4 GHz–6.1 GHz), and (6.8 GHz–9.9 GHz), respectively. The demonstrated antenna with quad notched bands achieves a good impedance matching at the 2.45 GHz ISM band.

It can be noted that the entire UWB resonance bandwidth is rejected by employing the proposed notches. Furthermore, both the measured and simulated results shown in Figure 10 present a narrow resonance band at the ISM band (2.27–2.57 GHz). The results illustrate measured S_{11} of -23.45 dB at the ISM band. This is because the current on the metal plate of a square monopole is concentrated along the outer edges of the radiating plate [15]. Therefore, the meander-line strip is placed on the upper edge of the radiated patch to achieve a high rejection quality (VSWR > 2) at the notched band. Furthermore, the strip increases the total length of radiation patch L. The length L improves the antenna and its width at the lower resonance frequency F_L of the proposed design. Both L_s and Z_s of

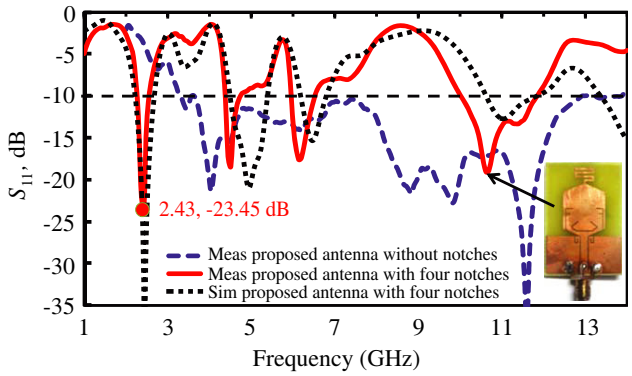

Figure 10. Measured return loss validation.

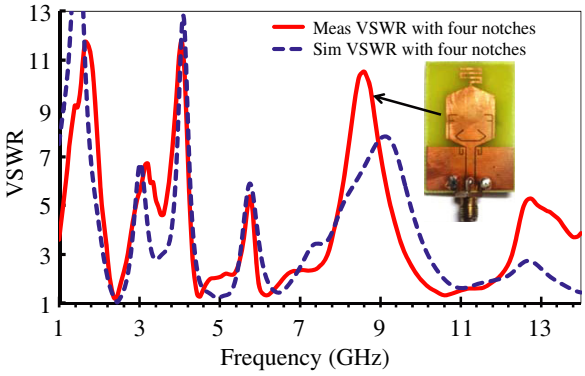

Figure 11. Measured and simulated VSWR.

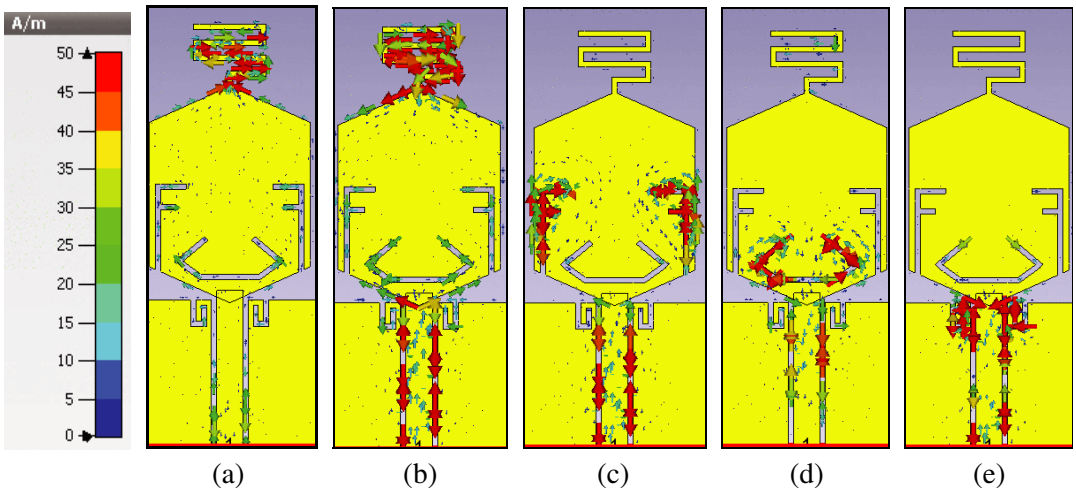

Figure 12. The current destruction, (a) 2.45 GHz, (b) 3 GHz, (c) 4.1 GHz, (d) 5.8 GHz, (e) 9 GHz.

the meander-line strip are adjusted to achieve resonance at the ISM band and reject the WiMAX band.

Figure 12 illustrates the simulated current distribution on the proposed antenna using CST software. Figure 12(a) and Figure 12(b) show high current density around the meander-line strip at 2.45 GHz, the resonance band, and at 3 GHz, the rejected band. The figures prove the two functions of the hybrid meander-line strip. Figures 12(c), 12(d), and 12(e) confirm the functionality of the F-slot, diamond-slot, and J-slot. The three figures display that the highest current is concentrated around the notches at 4 GHz, 5.75 GHz, and 9 GHz, respectively. A high current is distributed between the feed line edge and the ground plane for all the rejected bands.

The demonstrated antenna gain and radiation efficiency are presented in Figure 13. An acceptable gain between 2 dB and 6.4 dB for all the antenna bandwidths is observed by simulating the proposed antenna without notches. However, the four notches provide negative peak gains of −3.5 dB, −8 dB, −6 dB, and −4.1 dB at the rejected bands of the antenna. These results prove that the proposed antenna radiation is omitted at the four rejected bands. Moreover, the result shows a 1.54 dB gain at the ISM band. The radiated power of the proposed antenna achieves 0.439 W by setting the input power to 0.5 W at 2.45 Hz. Therefore, the antenna radiated-efficiency of 87.8% is calculated at the ISM band. This efficiency agrees with the simulated antenna efficacy in Figure 13, which shows 88% at the ISM band. However, the radiation efficiency is dropped at the rejected bands.

The measured and simulated normalised electric field (dBμV/m) radiation patterns at 2.45 GHz and 5 GHz are illustrated in Figure 14. The patterns show that the tested prototype has omnidirectional H-plane of co-polarisation radiation at the two tested frequencies. The E-plane co-polarisation patterns

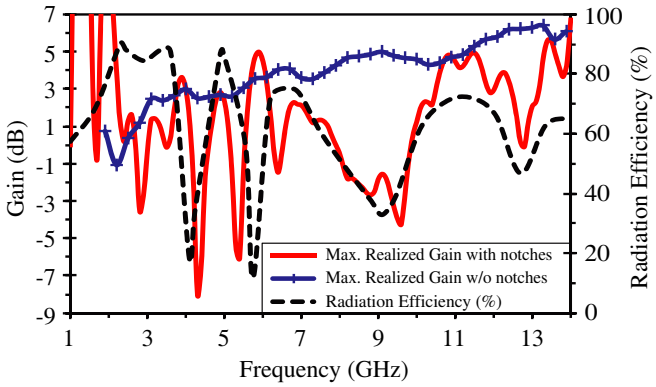

Figure 13. Gain (dB) and radiation efficiency.

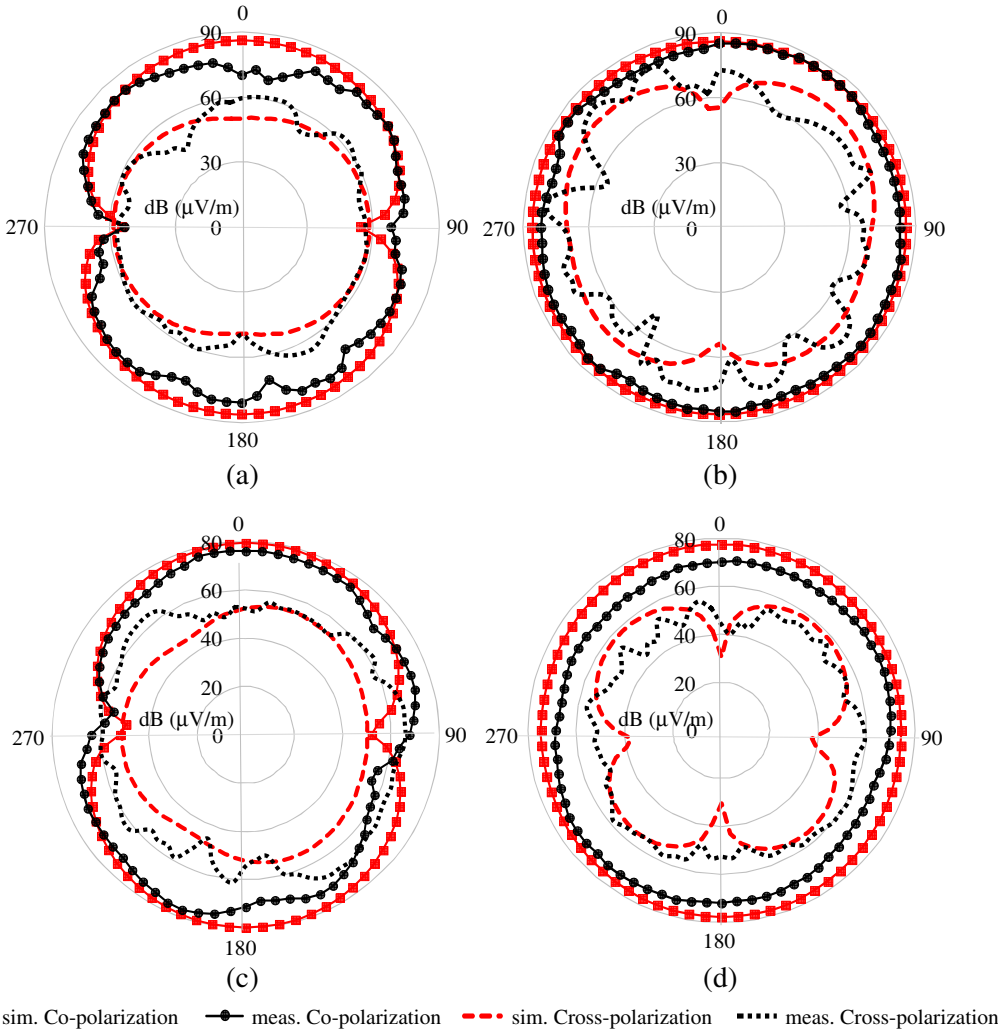

Figure 14. The measured (black colour) and simulated (red colour) antenna patterns, (a) 2.45 GHz E-plane, (b) 2.45 GHz H-plane, (c) 5 GHz E-plane, (d) 5 GHz H-plane, (cross - - - - -, co ——).

exhibit two bends at 90° and 270° of the measured frequencies. These results are matched with the characteristics of the monopole antenna. Conversely, the E-plane cross-polarisation patterns display a low electric-field level. On the other hand, the H-plane cross-polarisation patterns show a slightly

higher electric-field level with some ripples. Furthermore, the normalised simulation patterns agreed with the tested radiation patterns.

In summary, loading any notch shape on the antenna generates additional impedance Z_{notch} to the total antenna impedance Z_a. The notch impedance has a real part and imaginary part. Based on the notch structure and position, the notch can resonate at the operating frequency, and its impedance combines with the antenna input impedance. The additional impedance Z_{notch} makes the antenna mismatching (rejection band) or matching (resonance band) with input impedance at the operating frequency of the notch.

6. CONCLUSION

A compact UWB patch antenna with quad notched-bands is presented in this paper. The method combines mender-line strip, couple of F-slots, inverted diamond-slot, and pair of J-slots on a UWB antenna to reject four bands at 3 GHz, 4 GHz, 5.8 GHz, and 9 GHz. Furthermore, the antenna achieves a further resonance band of 2.27–2.57 GHz for ISM applications. The proposed antenna having an FBW of 133% is mostly rejected by the quad notches. The antenna radiation patterns are bi-directional in E-plane and omnidirectional in H-plane with an acceptable gain at the ISM band. The measured data and simulated results present a good agreement.

ACKNOWLEDGMENT

The authors are thankful to the Universiti Tun Hussein Onn Malaysia for sponsoring this work by office research and innovation (ORICC) grant (GPPS) Vote U464 and the Centre for Graduate Studies.

REFERENCES

1. Taki, H., S. Azou, A. Hamie, A. Al Housseini, A. Alaeddine, and A. Sharaiha, "On phaser-based processing of impulse radio UWB over fiber systems employing SOA," *Optical Fiber Technology*, Vol. 36, 33–40, 2017.
2. Boutejdar, A. and W. Abd Ellatif, "A novel compact UWB monopole antenna with enhanced bandwidth using triangular defected microstrip structure and stepped cut technique," *Microwave and Optical Technology Letters*, Vol. 58, No. 6, 1514–1519, 2016.
3. Ali, W. A., A. I. Zaki, and M. H. Abdou, "Design and fabrication of rectangular ring monopole array with parasitic elements for UWB applications," *Microwave and Optical Technology Letters*, Vol. 58, No. 9, 2268–2273, 2016.
4. Abdulhasan, R. A., R. Alias, A. Awaleh, and A. Mumin, "Design of circular patch microstrip ultra wideband antenna with two notch filters," *International Conference on Computer, Communications, and Control Technology (I4CT)*, 464–467, IEEE, Sarawak, Malaysia, Apr. 21–23, 2015.
5. Li, G., H. Zhai, T. Li, X. Y. Ma, and C.-H. Liang, "Design of a compact UWB antenna integrated with GSM/WCDMA/WLAN bands," *Progress In Electromagnetics Research*, Vol. 136, 409–419, 2013.
6. Vyas, K., A. K. Sharma, and P. K. Singhal, "Design and analysis of two novel CPW-fed dual band-notched UWB antennas with modified ground structures," *Progress In Electromagnetics Research C*, Vol. 49, 159–170, 2014.
7. Su, J., W. Ren, F. Lin, and X. Zhang, "A small UWB antenna with triple band-notched characteristics," *IEEE International Conference on Microwave and Millimeter Wave Technology (ICMMT)*, 280–282, IEEE, Beijing, China, Jun. 5, 2016.
8. Singh, P., A. R. Khanna, and H. Singh, "UWB antenna with dual notched band for WiMAX and WLAN applications," *Microwave and Optical Technology Letters*, Vol. 59, No. 4, 792–797, 2017.
9. Labade, R. P., S. B. Deosarkar, and N. Pisharoty, "Compact integrated bluetooth UWB antenna with quadruple bandnotched characteristics," *International Journal of Electrical and Computer Engineering (IJECE)*, Vol. 5, No. 6, 1433–1440, 2015.

10. Bakariya, P. S., S. Dwari, and M. Sarkar, "Printed ultrawideband monopole antenna with four notch band," *Wireless Personal Communications*, Vol. 84, No. 4, 2989–2999, 2015.
11. Sarijari, M. A., A. Lo, M. S. Abdullah, S. H. De Groot, I. G. Niemegeers, and R. A. Rashid, "Coexistence of heterogeneous and homogeneous wireless technologies in smart grid-home area network," *19th IEEE International Conference on Parallel and Distributed Systems (ICPADS)*, 576–581, IEEE, Seoul Korea, Dec. 15–18, 2013.
12. Donelli, M. and P. Febvre, "An inexpensive reconfigurable planar array for Wi-Fi applications," *Progress In Electromagnetics Research C*, Vol. 28, 71–81, 2012.
13. Viani, F., L. Lizzi, M. Donelli, D. Pregnolato, G. Oliveri, and A. Massa, "Exploitation of parasitic smart antennas in wireless sensor networks," *Journal of Electromagnetic Waves and Applications*, Vol. 24, No. 7, 993–1003, 2010.
14. Ray, K., "Design aspects of printed monopole antennas for ultra-wide band applications," *International Journal of Antennas and Propagation*, Vol. 2008, No. 713858, 1–8, 2008.
15. Ma, T.-G. and S.-J. Wu, "Ultrawideband band-notched folded strip monopole antenna," *IEEE Transactions on Antennas and Propagation*, Vol. 55, No. 9, 2473–2479, 2007.